Letter

Dynamical Born effective charges

C.-Yu Wang [1,2] S. Sharma [3] E. K. U. Gross [2] and J. K. Dewhurst [1,*]

[1]*Max-Planck-Institut für Mikrostrukturphysik, Weinberg 2, D-06120 Halle, Germany*

[2]*Fritz Haber Center for Molecular Dynamics, Institute of Chemistry, The Hebrew University of Jerusalem, Jerusalem 91904, Israel*

[3]*Max-Born-Institute for Nonlinear Optics and Short Pulse Spectroscopy, Max-Born Strasse 2A, 12489 Berlin, Germany*

(Received 11 August 2022; accepted 9 November 2022; published 16 November 2022)

We extend the definition of the Born effective charge to the dynamical regime. This is equal to the Fourier transform of the total electronic current divided by the Fourier transform of the velocity of a particular nucleus. The usual static Born effective charges are recovered in the zero-frequency limit. We calculate these charges for a selection of materials using time-dependent density functional theory in an all-electron code where the nuclei move along a chosen trajectory. A rich response function emerges with prominent resonance peaks. The finite value for the Born effective charge of metals is also reproduced. The dynamical Born effective charges are thus a natural choice of observable for probing the fundamental nonadiabatic coupling of electrons and nuclei.

DOI: 10.1103/PhysRevB.106.L180303

I. INTRODUCTION

The Born effective charge (BEC) is a useful and precisely defined quantity for both molecules and solids and one which can be both readily calculated and experimentally measured [1,2]. There are two equivalent definitions for the BEC: The first is the change in the electrostatic force $\mathbf{F}_\alpha$ on a nucleus α with respect to an external electric field $\mathbf{E}$,

$$Z^*_{\alpha ij} \equiv -\frac{\partial F_{\alpha i}}{\partial E_j}, \tag{1}$$

where i and j label Cartesian directions. The second, equivalent definition of the BEC is the change in the electric polarization of the system with respect to an infinitesimal displacement of a nucleus,

$$Z^*_{\alpha ij} \equiv Z_\alpha \delta_{ij} + \frac{\partial P_i}{\partial u_{\alpha j}}, \tag{2}$$

where Z_α is the nuclear charge, $\mathbf{P}$ is the electronic polarization, and $\mathbf{u}_\alpha$ is the displacement away from equilibrium. (We will follow the convention of taking the electronic charge e as $+1$ and the nuclear charges as negative.) For a finite system, the electronic polarization can be calculated using

$$\mathbf{P} = \int d^3r\, \rho(\mathbf{r})\mathbf{r}, \tag{3}$$

where ρ is the electronic charge density. For charge-neutral systems, the total polarization (one which includes the contribution from the nuclear charges) is independent of the choice of origin. On the other hand, the polarization of charge-neutral systems with periodic boundary conditions cannot be uniquely determined from Eq. (3). Instead, only the change in $\mathbf{P}$ can be calculated as a function of some parameter such as the external electric field or an atomic displacement [3–8]. This parameter may be made time dependent and the change in polarization determined from the adiabatic limit of the integrated electronic current. Let $\lambda(t)$ be the parameter as a function of time t and suppose that $\mathbf{J}(t)$ is the induced current. Then the change in polarization is given by

$$\Delta\mathbf{P} = \int_0^T dt\, \mathbf{J}(t). \tag{4}$$

The adiabaticity or "slowness" of the process is usually captured by representing the time dependence of the parameter by setting $\lambda(t) = f(t/T)$ with a function f which is bounded in the interval [0,1]. The adiabatic limit is then obtained by taking $T \to \infty$. It was shown by King-Smith and Vanderbilt [5] that the change in polarization is closely related to the Berry phase [9], and we will refer to their algorithm for calculating the static BEC as the "Berry phase method."

In its basic definition, the BEC is a static quantity evaluated from the adiabatic limit of the current. However, this definition can be easily and naturally extended to the nonadiabatic case in which the nucleus is moving at finite velocity along a prescribed path. The electronic current will respond accordingly and its frequency components can be determined. For what follows, we will restrict our attention to solids and also assume a noninteracting system of electrons in an effective Kohn-Sham [10,11] potential within the framework time-dependent density functional theory (TDDFT) [12].

Now choose $\lambda(t)$ to be the time-dependent displacement of nucleus α away from equilibrium $\mathbf{u}_\alpha(t)$, with $\mathbf{v}_\alpha(t) = \partial\mathbf{u}_\alpha(t)/\partial t$ as its velocity. The time-dependent total electronic current across a unit cell is given by

$$\mathbf{J}(t) = \frac{1}{N_k}\sum_{i\mathbf{k}}^{\text{occ}} \int d^3r\, \text{Im}[\varphi^*_{i\mathbf{k}}(\mathbf{r},t)\nabla\varphi_{i\mathbf{k}}(\mathbf{r},t)], \tag{5}$$

where $\varphi_{i\mathbf{k}}$ is the ith Kohn-Sham state at a particular k point in a set of N_k points, the sum is over the occupied states, and the integral is over the unit cell. We define the *dynamical Born*

*dewhurst@mpi-halle.mpg.de

effective charge (dynBEC) as a natural extension of Eq. (2),

$$Z^*_{\alpha ij}(\omega) \equiv Z_\alpha \delta_{ij} + \frac{\partial J_i(\omega)}{\partial v_{\alpha j}(\omega)}, \tag{6}$$

where

$$\mathbf{J}(\omega) \equiv \int_0^\infty dt\, \mathbf{J}(t) \exp[i(\omega + i\eta)t] \tag{7}$$

is the Fourier transform of the current, $\mathbf{v}_\alpha(\omega)$ the Fourier transform of the velocity, and η is a positive infinitesimal. Note that $\Delta\mathbf{P} = \Delta\mathbf{J}(\omega \to 0)$ and that the acoustic sum rule [13],

$$\sum_\alpha Z^*_{\alpha ij}(\omega \to 0) = 0, \tag{8}$$

is satisfied in the static limit owing to charge neutrality, although this is not true in general for all frequencies. This property is a useful indicator for establishing the quality of the numerical calculations.

The optical conductivity σ_{ij} can be calculated in the same manner from the current and the electric field,

$$\sigma_{ij}(\omega) = \frac{1}{\Omega} \frac{\partial J_i(\omega)}{\partial E_j(\omega)}, \tag{9}$$

where Ω is the unit cell volume, which implies that $\mathbf{u}_\alpha(t)$ is the analog of the vector potential $\mathbf{A}(t)$ and $\mathbf{v}_\alpha(t)$ is the analog of the electric field $\mathbf{E}(t) = -(1/c)\partial\mathbf{A}(t)/\partial t$.

Recently, the frequency-dependent generalization of the BEC was defined independently by Binci *et al.* [14] and Dreyer *et al.* [15]. However, in these works, $Z^*(\omega)$ was evaluated either at phonon frequencies or in the zero-frequency limit. In our work, we explore this quantity over an energy range from zero up to ∼100 eV.

II. IMPLEMENTATION

We implemented the dynBEC in the solid-state, all-electron code ELK [16] which uses linearized augmented plane waves (LAPWs) as a basis [17]. This basis depends parametrically on the nuclear coordinates, which complicates the time evolution of the combined electronic and nuclear systems. Let V_{ext} be the external potential consisting of the Coulomb potential of the bare nuclei. Rather than explicitly moving the nuclei, we instead modify the external potential with

$$V_{\text{ext}}(\mathbf{r}, t) = V_{\text{ext}}(\mathbf{r}) - \mathbf{u}_\alpha(t) \cdot \boldsymbol{\nabla}_\alpha V_{\text{ext}}(\mathbf{r}), \tag{10}$$

where $\boldsymbol{\nabla}_\alpha$ is the derivative with respect to the displacement $\mathbf{u}_\alpha$. This approach is only valid for small displacements of the nuclei and, in fact, our investigation into the BEC began as a means of evaluating the validity of this approximation. In practice, we also add the derivative of the Coulomb (i.e., Hartree) potential of the core electrons, which are not included in the TDDFT dynamics, under the assumption that the core electrons move rigidly with the nuclei and serve to screen the Coulomb potential of the nuclei. Note that, in principle, the contribution from the exchange-correlation potential of the core electrons should be included in the gradient of the potential in Eq. (10). However, owing to the nonlinearity of the exchange-correlation potential with respect to the density, it is not possible to uniquely extract that part of the potential which arises from the core electrons alone. We discovered, however, that this contribution to the gradient had a negligible effect on the results and chose instead to omit it.

The real-time dynamics were performed using a scheme in which the time-dependent Kohn-Sham orbitals are expanded in the eigenvectors of the instantaneous Hamiltonian and propagated using phase factors over a small time interval [18].

The dynBEC as defined in Eq. (6) is independent of the choice of path. This is because of the linearity of response functions in general: One can apply an atomic displacement either of a single frequency or multiple frequencies together. Both will yield the same response function because the frequency response decouples in the linear regime. The choice of frequencies and their amplitudes defines a particular path in time and, because we divide by the velocity in Eq. (6), the dynBEC is independent of this choice. The only proviso is that any path should contain a nonzero component from each frequency.

For convenience, we choose an *instantaneous displacement* at $t = 0$. The corresponding velocity is therefore a δ function in time whose Fourier transform is a constant. This removes the need to divide by $v_{\alpha j}(\omega)$ in Eq. (6) and thus eliminates a source of numerical error. It is important to note that the dynBEC is part of the general response function,

$$\chi(\mathbf{r}, \mathbf{r}', t - t') \equiv \frac{\delta\rho(\mathbf{r}, t)}{\delta V_{\text{ext}}(\mathbf{r}', t')}. \tag{11}$$

In our case, we take δV_{ext} to be the change in external potential caused by the displacement of a nuclei given in Eq. (10). One may ask whether the Kohn-Sham system which reproduces the exact density also yields the exact total current, as required by Eq. (6). In general, the first-order response of the macroscopic current $\delta\mathbf{J}$ is exact even though the Kohn-Sham current density $\mathbf{j}(\mathbf{r})$ is not [19]. This is a consequence of the continuity equation applied to the long-range response of the density (see, also, Eqs. (1.20), (A2), and (A3) of Ref. [20]). Thus, TDDFT is sufficient for calculation of the dynBEC for periodic systems.

The full response function can be evaluated from the Kohn-Sham response function χ_s using the Dyson equation in frequency space [21],

$$\chi(\mathbf{r}, \mathbf{r}', \omega) = \chi_s(\mathbf{r}, \mathbf{r}', \omega) + \int d^3r_1\, d^3r_2\, \chi_s(\mathbf{r}, \mathbf{r}_1, \omega)\left[\frac{1}{|\mathbf{r}_1 - \mathbf{r}_2|} + f_{\text{xc}}(\mathbf{r}_1, \mathbf{r}_2, \omega)\right]\chi(\mathbf{r}_2, \mathbf{r}', \omega), \tag{12}$$

where f_{xc} is the exchange-correlation kernel. We can write the change in total electronic current corresponding to the Kohn-Sham response function explicitly as follows [6,15,22–24]:

$$\frac{\partial \mathbf{J}_s(\omega)}{\partial v_{\alpha j}(\omega)} = \frac{i}{\omega} \sum_{\mathbf{k}} \sum_i^{\text{occ}} \sum_j^{\text{unocc}} \left[\frac{\langle\varphi_{i\mathbf{k}}|\hat{\mathbf{p}}|\varphi_{j\mathbf{k}}\rangle\langle\varphi_{j\mathbf{k}}|\partial\hat{V}_{\text{ext}}/\partial u_{\alpha j}|\varphi_{i\mathbf{k}}\rangle}{\varepsilon_{j\mathbf{k}} - \varepsilon_{i\mathbf{k}} + \omega + i\eta} + \text{c.c.}(\omega \to -\omega)\right]. \tag{13}$$

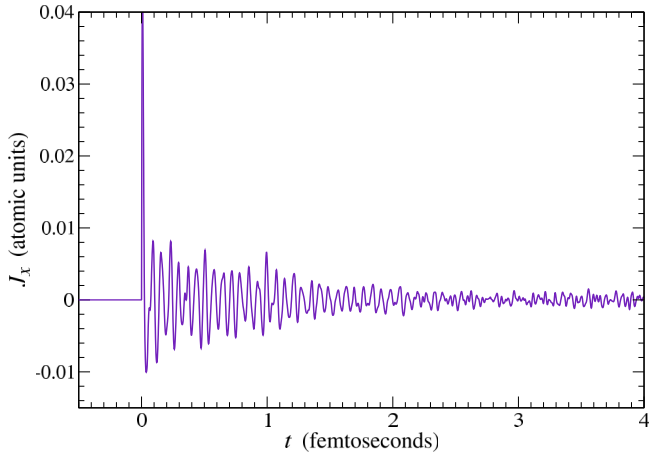

FIG. 1. Time-dependent electronic current across a single unit cell of LiF after a small, instantaneous displacement of the Li nucleus in the x direction at $t = 0$. The total simulation time was 19.4 femtoseconds.

This formula does not, however, include the self-consistent change in the Kohn-Sham potential arising from the change in density. To incorporate this effect, the full Kohn-Sham response function χ_s should be calculated and then used in Eq. (12) along with $f_{\rm xc}$. Our approach of performing a real-time TDDFT is equivalent to this, but numerically more convenient. This is because solving the Dyson equation with sufficient spatial resolution for the derivative of the Coulomb potential in Eq. (10) would be prohibitively expensive for an all-electron method.

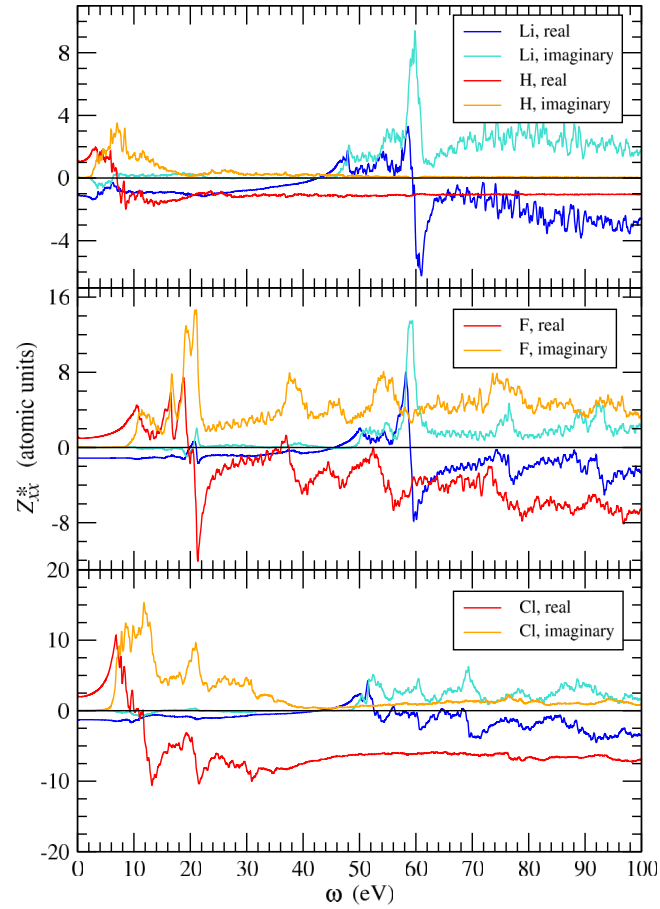

FIG. 2. Dynamical Born effective charges of LiH (top), LiF (center), and LiCl (bottom).

III. RESULTS

The code was used to find the dynBEC of the ionic polar insulators LiH, LiF, and LiCl, the covalently bonded BN in both the cubic and hexagonal phases, the nonpolar insulator diamond, and the fcc metal Al. The materials were chosen to demonstrate some distinct characteristics of the dynBEC and, because their constituent atoms are fairly light, lessen the computational expense. In Fig. 1, we plot the current generated by instantaneously displacing the Li nucleus at $t = 0$ in LiF. This is typical of the behavior of the current obtained for all the materials and nuclei, namely, a large initial spike in current followed by rapid and varied oscillations. In the case of Li, the amplitude of the oscillations decreased until around 3 femtoseconds and then reached a "steady state." Total simulation time for all our calculations was 800 atomic units of time, or 19.4 femtoseconds. Each time step for the simulations was 1.2 attoseconds. This current was then numerically Fourier transformed with η in Eq. (7) taken to be 0.136 eV (except in the case of Al, where various values were tested). The static BEC results for all the materials are collated in Table I.

The dynBEC of the ionic compounds LiH, LiF, and LiCl is plotted in Fig. 2. This is a complex quantity and so the

TABLE I. Static Born effective charges of various materials calculated from the $\omega \to 0$ of the dynBEC compared to those calculated with the Berry phase method and experiment. The units of charge are e, i.e., the electronic charge. The value in parentheses is the average of the two absolute values.

		Experiment	Berry [5,16]	$Z^*(\omega \to 0)$		
LiH		0.991 [26,27]	1.04	Li: −1.03	H: 1.13	(1.08)
LiF		1.045 [27,28]	1.05	Li: −1.11	F: 1.12	(1.11)
LiCl		1.231 [27,28]	1.18	Li: −1.35	Cl: 2.06	(1.70)
cubic BN		1.98 [29,30]	1.89	B: −1.57	N: 1.97	(1.77)
hexagonal BN	x		2.72	B: −2.28	N: 3.05	(2.67)
	z		0.75	B: −0.44	N: 1.07	(0.76)
Al					−2.09	
diamond					−0.15	

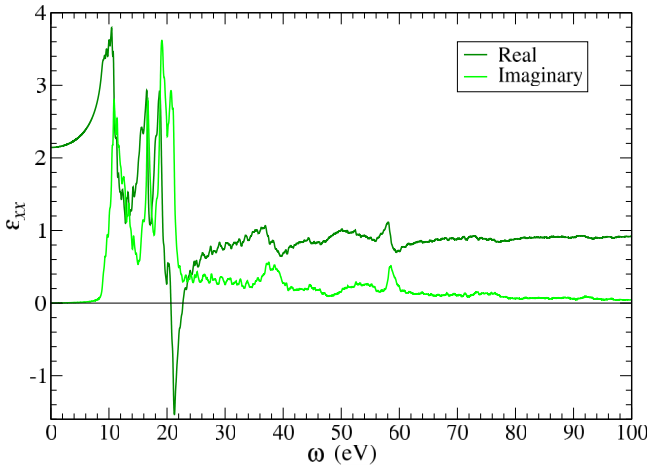

FIG. 3. Dielectric function of LiF calculated within the RPA.

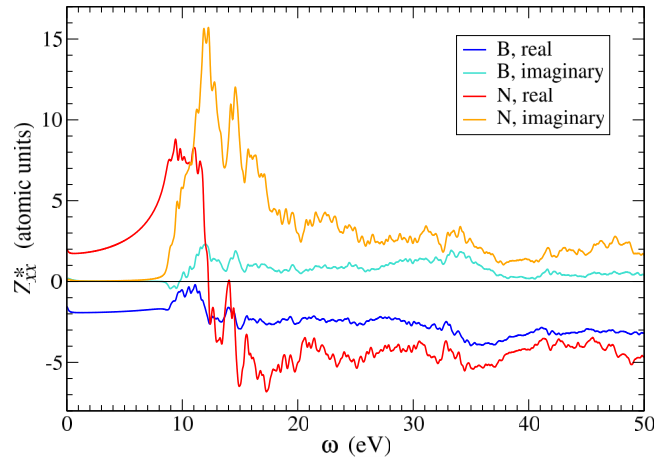

FIG. 4. Dynamical Born effective charges of cubic BN.

real and imaginary parts are plotted separately. In the limit as $\omega \to 0$, the real part of the dynBEC tends to the regular static BEC, although the acoustic sum rule, given by Eq. (8), is not perfectly satisfied. This may be due to the incompleteness of the LAPW basis, particulary when expanding the change in wave function owing to an atomic displacement simulated with Eq. (10). The error can be reduced by increasing the size of the basis used for the time evolution of the Kohn-Sham orbitals, but ultimately becomes numerically unfeasible. The best case is that of LiF (Li: −1.11, F: 1.12) and the worst is LiCl (Li: −1.35, Cl: 2.06). However, the sum rule itself can be used to partially correct this error by taking an average of absolute values for our two atom systems.[1] The resulting charges are then in good agreement with the Berry phase method and experiment. An exception is that of LiCl for which the BEC of Li is in relatively good agreement with that of the Berry phase method, however the value for Cl is too large. This gives an average value of 1.70, which is over 40% greater than it should be. Unfortunately, we were unable to converge this calculation any further.

The dynBEC of the covalently bonded boron nitride in both the cubic and hexagonal phases is shown in Figs. 4 and 5. The zero-frequency limit gave good agreement for the static BEC with that of the Berry phase method and, for the cubic case, experiment. Notably, the BEC for the x and z directions of hBN are significantly different and yet the two methods are in excellent agreement for both. Diamond, which is also covalently bonded but not a polar semiconductor, should give a BEC of zero. Our result for the zero-frequency limit of the dynBEC is −0.15. This slight discrepancy may again be due to the limitation of the LAPW basis.

The metallic case is the most interesting as far as the static limit is concerned. Until recently, it was assumed that the BEC for metals was undefined. However, Dreyer *et al.* [15] showed that this is not the case and demonstrated that there is a nonadiabatic version of the BEC for metals and related it to the Drude weight. The dynBEC of Al for small frequencies is plotted in the inset of Fig. 7. One can see that the value taken for η affects the $\omega \to 0$ limit. There are noticeable oscillations in the plots calculated with small values of η. For comparison, the dielectric function ϵ_{xx}, calculated within the random phase approximation (RPA), is plotted in Fig. 8 with and without the intraband term [25]. Using the same k-point set as that for the dynBEC (42 × 42 × 42), the oscillations in ϵ_{xx} mirror those in the dynBEC. A much denser set (72 × 72 × 72) removes the oscillations in the dielectric function, indicating that they are merely an artifact of a finite k-point grid. These oscillations can be suppressed either by increasing the number of k points or increasing the value of η. We find that taking $\eta = 0.544$ eV smooths the curve sufficiently without distorting the data. Using this value for η, our prediction for the nonadiabatic

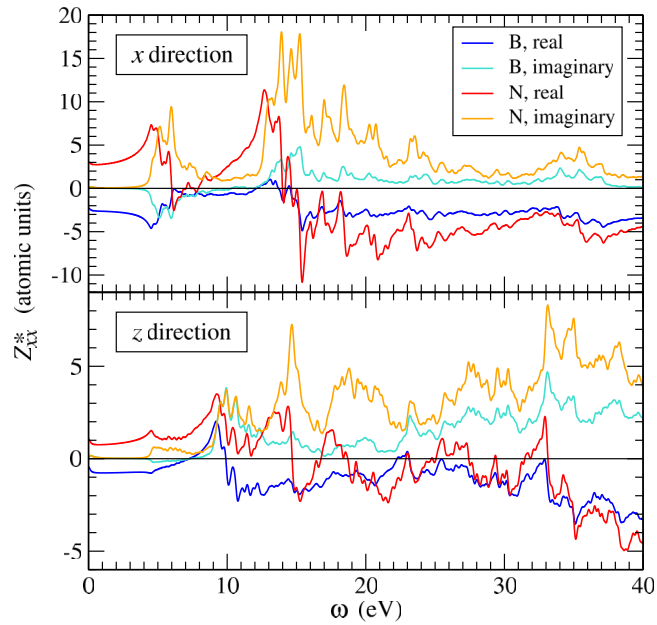

FIG. 5. Dynamical Born effective charges of hexagonal BN for the x and z directions.

[1]The static BEC determined from the Berry phase method could be used to further correct numerical inaccuracies in the dynBEC by adding a real constant to $Z^*(\omega)$ so that the two methods are in agreement at $\omega = 0$. The imaginary part of the dynBEC could then be calculated using a Kramers-Kronig transformation.

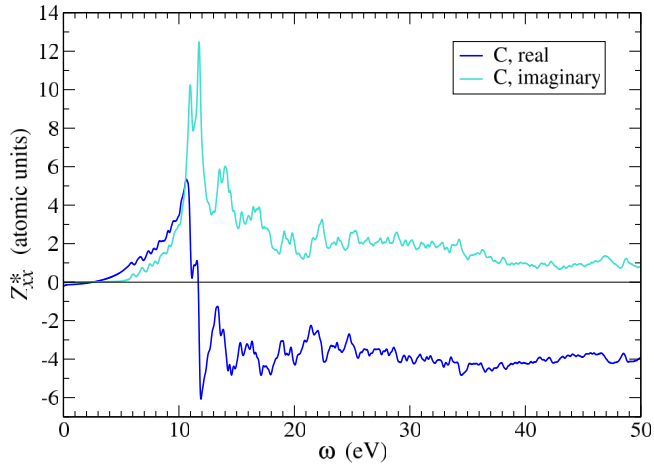

FIG. 6. Dynamical Born effective charges of diamond.

BEC is −2.09, which is in excellent agreement with the value of −2.0 determined by Dreyer *et al.*

At finite frequencies, the dynBEC spectral functions of each atom are very different. In the case of LiX, the imaginary part of the dynBEC for Li is zero until about 50 eV, whereas the onset for H, F, and Cl is much lower, ranging from 3 to 8 eV. There are also several prominent resonant peaks. In LiH and LiF, a clear resonance in the Li part of the spectrum can be seen around 60 eV. At this point, the real part crosses the zero axis and the imaginary part has a sharp peak. This peak corresponds to a transition between the Li 1*s* and 2*p* orbitals. It is almost completely absent in LiCl because the 2*p* state is considerably more hybridized. Aside from the conspicuous resonances, the Li dynBEC is noticeably dissimilar for the three compounds throughout the entire range of frequencies, despite the fact that the materials have the same crystal structure and same type of bonding. This suggests that the dynBEC is highly sensitive to the chemical environment of the selected atom.

There are also axis crossings of the real part of the dynBEC for H, F, and Cl. The corresponding peaks in the imaginary parts are not as well defined as those for Li. The most pronounced is that of F with a resonance around 20 eV.

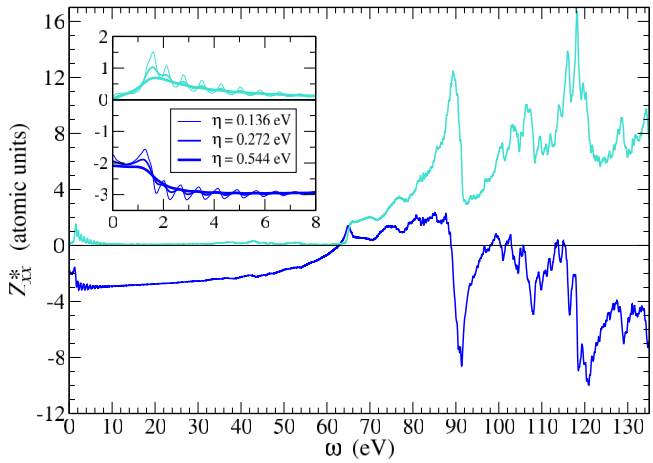

FIG. 7. Dynamical Born effective charge of Al. The inset shows the low-frequency behavior of the dynBEC for three different values of η used in Eq. (7).

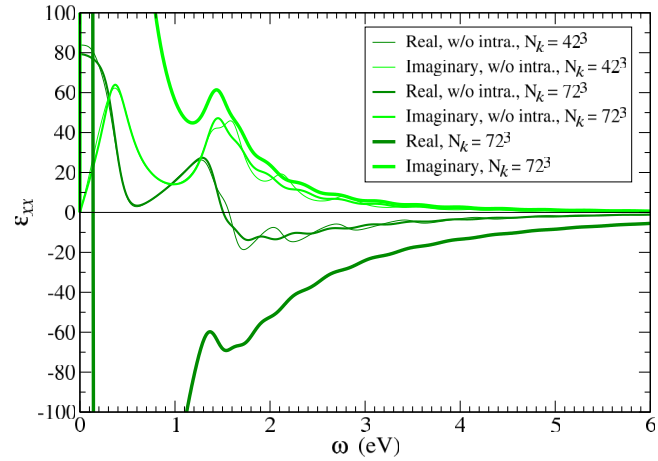

FIG. 8. Dielectric function of Al calculated within the RPA. The plot contains ϵ_{xx} with and without the intraband "Drude" term. Also included is the dielectric function calculated on the same k-point grid as that used for the dynBEC calculation.

Comparing the dynBEC of LiF to its dielectric function in Fig. 3 reveals similarity in the positions of the most prominent peaks, particularly for lower energies (<20 eV) and for the fluorine part. This is not surprising because peak positions are largely dictated by the denominator in the noninteracting response function given by Eq. (13). What is different are the relative weights of the peaks owing to the difference in the matrix elements in the numerator. Furthermore, the dynBEC retains its relative amplitude even for high energies where ϵ_{xx} has tapered off. The reason is that δV_{ext} acts more strongly on orbitals bound closely to the nuclei than does a spatially constant external electric field. Thus, higher-energy excitations will have higher weights for the dynBEC.

Turning to the finite-frequency dynBEC of the covalently bonded materials BN and diamond as shown in Figs. 4–6, we observe similarly intricate spectra. The peaks are generally broader, indicating increased hybridization between the atomic orbitals. Also noteworthy is the similarity of the dynBEC spectra of cBN and diamond at finite frequency, even though the static BECs are very different for these materials. Of particular significance is the distinction between the dynBEC for the x and z directions of hexagonal BN. Thus, not only does the dynBEC discriminate between different atoms, but also different directions.

Lastly, for the case of Al in Fig. 7, the spectrum is fairly featureless until 64 eV when there is a crossing of the axis by the real part and an onset of the imaginary part. After this, there are several prominent peaks in the spectrum, particularly at about 90 and 118 eV. Compared to the dielectric function in Fig. 8 in which ϵ_{xx} diverges because of the intraband term, the dynBEC is finite at $\omega = 0$. Thus, if the dynBEC can be measured experimentally, it should more suited than the dielectric function to resolve low-frequency features in the response function of metals.

IV. SUMMARY

We have extended the definition of the Born effective charge to a dynamical, frequency-dependent variant. This was

calculated using an instantaneous displacement of a nucleus and then performing a Fourier transformation of the resulting electronic current computed with TDDFT. The dynBEC is a natural extension to the regular static BEC and we anticipate that it may be measurable with neutron diffraction techniques [31]. Unlike the dielectric function, the dynBEC discriminates between atoms in the solid and thus is intimately connected to nonadiabatic coupling between nuclei and electrons. In effect, it quantifies the amount of electronic charge "dragged" along with a nucleus, when that nucleus is moving back and forth at a given frequency.

The primary utility of having an accurate experimental measurement of the dynBEC would be to determine any error in the theoretical prediction. Such a deviation would be due almost entirely to the approximation of the TDDFT kernel f_{xc} used in Eq. (12). For instance, the closely related dielectric function suffers from significant error for excitonic materials [32]. In these cases, the resonant excitonic peaks are not captured by the usual adiabatic approximations to f_{xc} and considerable theoretical effort has been expended in producing functionals which do work [33,34]. Are there similar limitations to using the adiabatic functionals for the prediction of the dynBEC? Comparison to experiment should be able to answer this and ultimately aid in the development of TDDFT functionals for the case of combined electron and nuclear dynamics [35]. Another potential use would be to improve first-principles calculations of ion stopping in condensed matter, particularly in the energy range of up to a few-hundred electron volts [36,37]. In this regime, so-called nuclear stopping dominates in which the ions' kinetic energy is primarily transferred to the nuclei. The dynBEC could quantify how much of this energy is subsequently absorbed by excitation of electronic currents. Lastly, molecular dynamics calculations within the adiabatic approximation but driven by a laser pulse given by a vector potential $\mathbf{A}(t)$ could utilize the dynBEC for determining the contribution to the force on each atom by the laser. The electric field is given by $\mathbf{E}(t) = -(1/c)d\mathbf{A}/dt$ and the force on atom α would be modified by $\mathbf{F}_\alpha(t) \to \mathbf{F}_\alpha(t) - Z^*_\alpha \mathbf{E}(t)$. The choice of the matrix Z^*_α as the effective charge which couples to the electric field arises from Eq. (1). However, with the dynamical BEC, one could match Z^*_α to the laser frequency, i.e., choose $Z^*_\alpha(\omega_{\mathrm{laser}})$ instead of $Z^*_\alpha(0)$, which should be the better choice in this situation.

ACKNOWLEDGMENTS

We would like to thank Vladimir Nazarov for useful discussions. Calculations were performed at the Max Planck Computing and Data Facility as well as at The Hebrew University of Jerusalem. S.S. and J.K.D. are thankful for the support of TRR227 (Project No. A04) for funding. E.K.U.G. would like to acknowledge the European Research Council (ERC) under the European Union's Horizon 2020 research and innovation programme (Grant Agreement No. ERC-2017-AdG-788890).

[1] M. Born and K. Huang, *Dynamical Theory of Crystal Lattices*, International Series of Monographs on Physics (Clarendon Press, Oxford, 1954).
[2] J. D. Axe, Phys. Rev. **157**, 429 (1967).
[3] S. Baroni, P. Giannozzi, and A. Testa, Phys. Rev. Lett. **58**, 1861 (1987).
[4] X. Gonze, D. C. Allan, and M. P. Teter, Phys. Rev. Lett. **68**, 3603 (1992).
[5] R. D. King-Smith and D. Vanderbilt, Phys. Rev. B **47**, 1651 (1993).
[6] R. Resta, Rev. Mod. Phys. **66**, 899 (1994).
[7] X. Gonze and C. Lee, Phys. Rev. B **55**, 10355 (1997).
[8] R. Resta and D. Vanderbilt, Theory of polarization: A modern approach, in *Physics of Ferroelectrics: A Modern Perspective*, edited by C. H. Ahn, J.-M. Triscone, and K. M. Rabe (Springer, Berlin, Heidelberg, 2007), pp. 31–68.
[9] M. V. Berry, Proc. R. Soc. London A **392**, 45 (1984).
[10] P. Hohenberg and W. Kohn, Phys. Rev. **136**, B864 (1964).
[11] W. Kohn and L. J. Sham, Phys. Rev. **140**, A1133 (1965).
[12] E. Runge and E. K. U. Gross, Phys. Rev. Lett. **52**, 997 (1984).
[13] R. M. Pick, M. H. Cohen, and R. M. Martin, Phys. Rev. B **1**, 910 (1970).
[14] L. Binci, P. Barone, and F. Mauri, Phys. Rev. B **103**, 134304 (2021).
[15] C. E. Dreyer, S. Coh, and M. Stengel, Phys. Rev. Lett. **128**, 095901 (2022).
[16] The Elk Code, http://elk.sourceforge.net/.
[17] D. Singh and L. Nordstrom, *Planewaves, Pseudopotentials, and the LAPW Method* (Springer, New York, 2006).
[18] J. Dewhurst, K. Krieger, S. Sharma, and E. Gross, Comput. Phys. Commun. **209**, 92 (2016).
[19] R. D'Agosta and G. Vignale, Phys. Rev. B **71**, 245103 (2005).
[20] S. L. Adler, Phys. Rev. **126**, 413 (1962).
[21] M. Petersilka, U. J. Gossmann, and E. K. U. Gross, Phys. Rev. Lett. **76**, 1212 (1996).
[22] F. Kootstra, P. L. de Boeij, and J. G. Snijders, J. Chem. Phys. **112**, 6517 (2000).
[23] F. Kootstra, P. L. de Boeij, and J. G. Snijders, Phys. Rev. B **62**, 7071 (2000).
[24] P. Romaniello and P. L. de Boeij, Phys. Rev. B **71**, 155108 (2005).
[25] M. Cazzaniga, L. Caramella, N. Manini, and G. Onida, Phys. Rev. B **82**, 035104 (2010).
[26] M. Brodsky and E. Burstein, J. Phys. Chem. Solids **28**, 1655 (1967).
[27] A. Shukla, Phys. Rev. B **61**, 13277 (2000).
[28] M. J. Sangster, R. M. Atwood, and U. Schroder, J. Phys. C **11**, 1523 (1978).
[29] J. A. Sanjurjo, E. López-Cruz, P. Vogl, and M. Cardona, Phys. Rev. B **28**, 4579 (1983).
[30] K. Shimada, T. Sota, and K. Suzuki, J. Appl. Phys. **84**, 4951 (1998).
[31] S. W. Lovesey, *Theory of Neutron Scattering from Condensed Matter* (Clarendon Press, Oxford, 1984).

[32] G. Onida, L. Reining, and A. Rubio, Rev. Mod. Phys. **74**, 601 (2002).
[33] S. Sharma, J. K. Dewhurst, A. Sanna, and E. K. U. Gross, Phys. Rev. Lett. **107**, 186401 (2011).
[34] Y.-M. Byun and C. A. Ullrich, Phys. Rev. B **95**, 205136 (2017).
[35] X. Li, J. C. Tully, H. B. Schlegel, and M. J. Frisch, J. Chem. Phys. **123**, 084106 (2005).
[36] P. Sigmund, Bull. Russ. Acad. Sci.: Phys. **72**, 569 (2008).
[37] M. Caro, A. A. Correa, E. Artacho, and A. Caro, Sci. Rep. **7**, 2618 (2017).